Electronic Supplementary Material (ESI) for Soft Matter.

Supplemental Materials: Field-theoretic Simulations of Random Copolymers with Structural Rigidity

Shifan Mao,[†] Quinn MacPherson,[‡] Jian Qin,[†] and Andrew J. Spakowitz[*,†,¶,§,‖,⊥]

†Department of Chemical Engineering, Stanford University, Stanford, CA, 94305

‡Department of Physics, Stanford University, Stanford, CA, 94305

¶Department of Applied Physics, Stanford University, Stanford, CA, 94305

§Department of Materials Science and Engineering, Stanford University, Stanford, CA, 94305

‖Biophysics Program, Stanford University, Stanford, CA, 94305

⊥Stanford Institute for Materials and Energy Sciences, SLAC National Accelerator Laboratory, 2575 Sand Hill Road, Menlo Park, CA 94025

E-mail: ajspakow@stanford.edu

Supplemental Materials

Degrees of Mixing and Heat Capacity for All Simulations

In Fig. 5 of our manuscript, we included only the data for rigid polymers. Here we include the plots for all three flexibilities for completeness. The data here was used to generate the phase diagrams in Figs. 3 and 4 of our manscript.

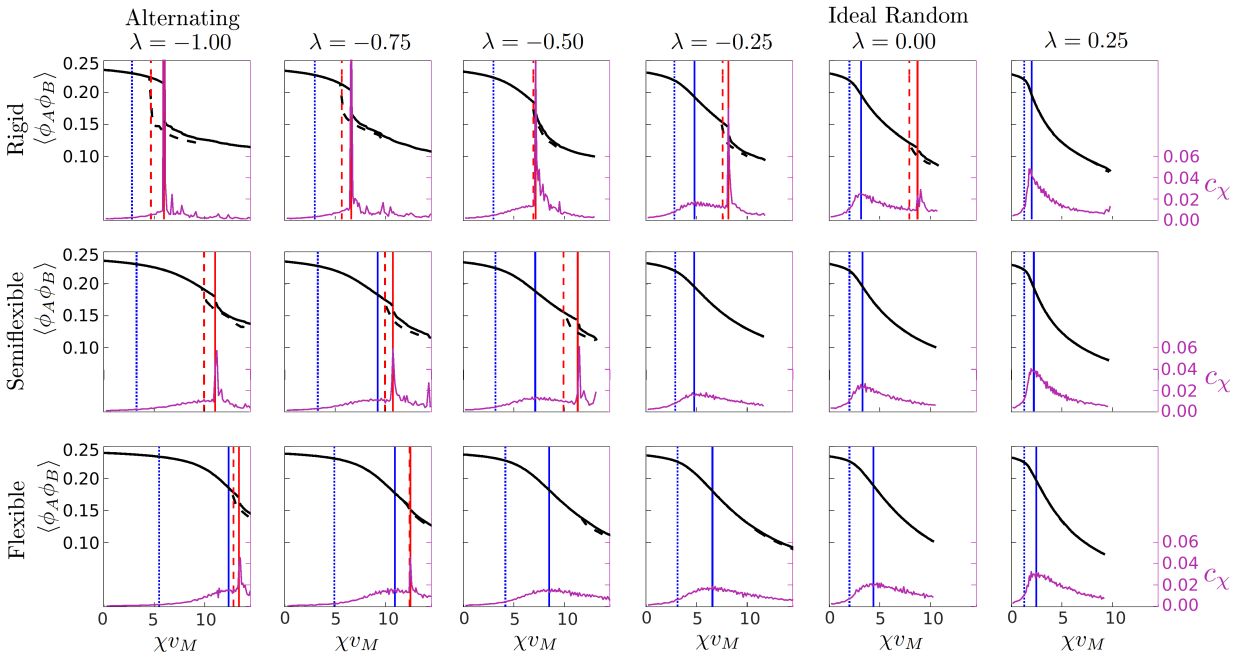

Figure 1: Extended version of Fig. 5 of our manuscript including all three flexibilities. Degree of mixing and heat capacity of rigid random copolymers. Each plot contains the degree of mixing $\langle \phi_A \phi_B \rangle$ (left y-axis) from simulated cooling to higher χv_M (solid black) and melting to lower χv_M (dashed black). In addition, the heat capacity c_χ (green, right y-axis) is shown in each plot. The vertical lines mark the χv_M value of the mean-field spinodal (dotted blue), the H-to-RM transition (solid blue), the AM-melting phase transition (dashed red), and the phase transition to the AM phase on cooling (solid red).

Single-chain Conformations

The name "Aligned Micro-phase" denoted as AM in phase diagrams in Figs. **??** and **??** derives from the orientational alignment of the polymers. We quantify the degree of polymer alignment using the eigenvalues of probability distribution of monomer end-to-end vectors.

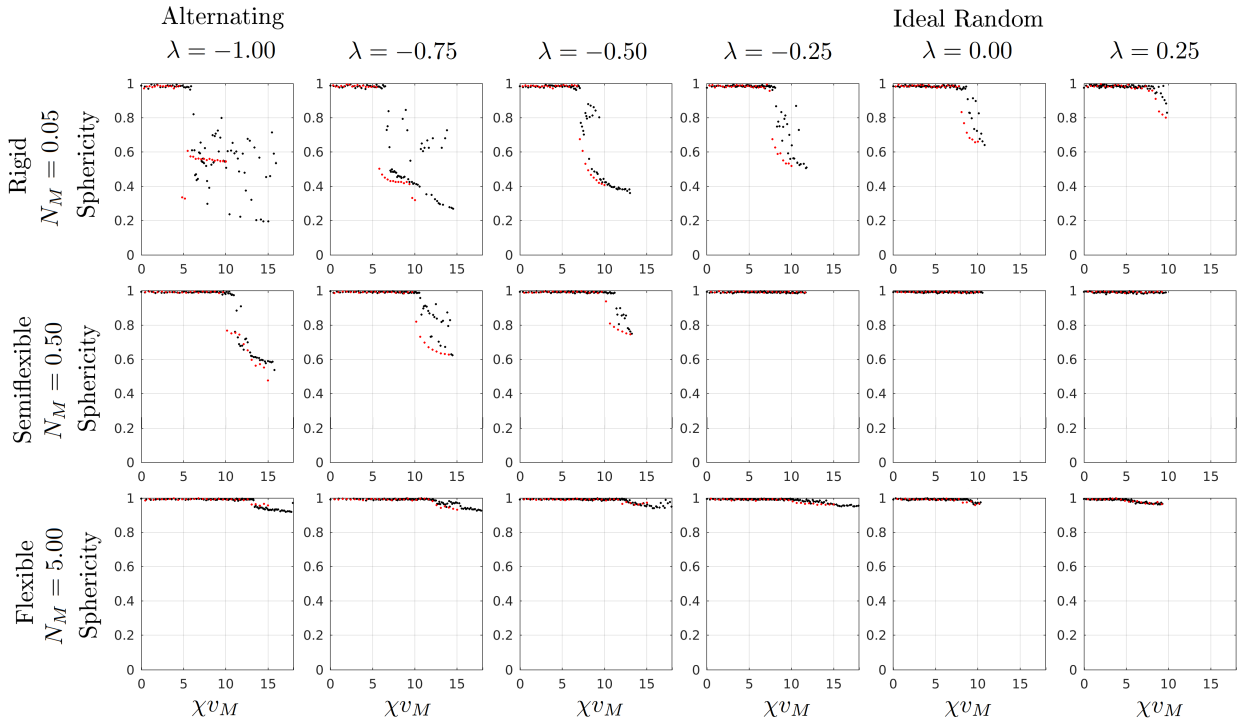

Figure 2: Sphericity, the degree of spherical symmetry of monomer end-to-end vectors, as a function of χv_M. A sphericity of 1 corresponds to uncorrelated orientations while a value of 0 corresponds to perfectly aligned ones. The black dots are drawn from cooling simulations with increasing χv_M, and the red dots are from melting simulations with decreasing χv_M simulations. This set of data is not ensemble averaged.

In particular, we look at sphericity S defined as

$$S = \frac{3}{2}(\lambda_2 + \lambda_3)$$

where $\lambda_1 \geq \lambda_2 \geq \lambda_3$ are the eigenvalues of the matrix

$$M_{ij} = \frac{\sum_m p_m^i p_m^j}{\sum_m \vec{p_m}^2}$$

where p_m^i is the ith component of the end-to-end vector of the m^{th} monomer. The sums are over all monomers in the melt for a particular simulation snapshot. The value of S ranges from zero for perfectly a aligned melt to one for a randomly oriented melt. Figure 2 shows the sphericity of snap shots drawn from the simulation under different χ, N_m, and

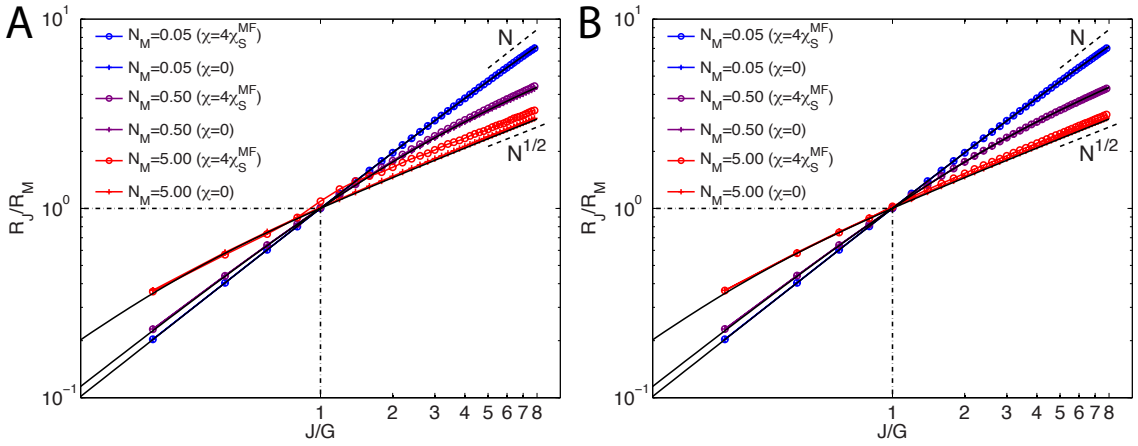

Figure 3: Chain segment length R_J/R_M versus segment rigidity ϵN at different monomer rigidities $N_M = 0.05, 0.50, 5.00$. Plot A and B show R_J/R_M for chemically anticorrelated polymers with $\lambda = -0.75$ and ideal random polymers with $\lambda = 0$ respectively. Black lines are unperturbed R_J/R_M, '+' symbols represent R_J/R_M at $\chi = 0$, and '∘' symbols R_J/R_M at $\chi = 4\chi_S^{MF}$.

λ values. At low χ values corresponding to the H phase, the sphericity is nearly 1. As one would expect, the lowest sphericity values are observed for rigid alternating polymers at high χ values. Rigid polymers have a lower entropic penalty to aligning their monomers in a particular direction and the alternating pattern along the polymer aligning to the lamellar density field is the driving force for alignment.

Note that there is considerable spread in sphericity in the AM phase for the increasing χ (Black) configurations. This is due to the dispersity of melt configurations, caused by segregation frustration. The sphericity values with decreasing χ simulations (red) do not show a spread, since they start from the same melt configuration at high χ.

Next we compare the single-chain conformational changes of rigid and flexible random copolymers throughout the phase transition in the melt. We first define chain segment length R_J as

$$R_J = \langle [\vec{r}(Jl_0) - \vec{r}(0)]^2 \rangle^{1/2}, \tag{1}$$

where bead index J runs from 0 to $MG - 1$, and the bracket indicates ensemble average over all chains and melt configurations. Figure 3 shows R_J/R_M versus monomer index J/G,

at different flexibility N_M and degree of chemical correlation λ = −0.75 (A) and λ = 0 (B). In Fig. 3, the corresponding black lines are the unperturbed segment lengths R_J/R_M. The '+' symbols represent R_J/R_M in the homogeneous phase at χ = 0 and circles are R_J/R_M at strong segregation at $\chi = 4\chi_{\rm S}^{\rm MF}$. The chains with different monomer flexibility show different scaling of R_J with respect to J/G. The chain conformation, at least by the metric R_J, remains largely unperturbed with only a modest stretching of the long distance behavior of flexible polymers in at strong segregation. The stretching of flexible polymers is more pronounced when monomers are chemically anticorrelated (λ=-0.75). As we have shown, anticorrelated polymers form lamellar structures at high χ values, the surface energy of which is likely responsible for the stretching. On the other hand, rigid polymers (N_M=0.05) remain in the unperturbed conformation throughout the phase transition at both chemical correlations.

Note that unlike traditional wormlike chain models,[1,2] in our simulation the stretching of rigid polymers are made possible by discrete shearable-stretchable wormlike chains with chain extension degree of freedom.[3,4]

These comparisons indicate that flexible polymers microphase segregate as a result of competition between surface free energy and extensional free energy, while rigid polymers phase segregation is due to competition between surface free energy and orientational entropy. The extension of flexible polymers also provides an explanation of the more pronounced shift of q^*, or the emergence of larger scale domain sizes of anticorrelated flexible polymers shown in Fig. 6C of our manuscript.

Chain Partitions

When chemical correlation is above the Lifshitz point $\lambda > \lambda_{\rm L}^{\rm MF}$, phase segregation is achieved by separating chains with different chemical compositions (fraction of A-type monomers in a single chain). To visualize such spatial partition of chains during phase segregation, we look at the snapshots of random copolymer melts composed of original chemical identities and

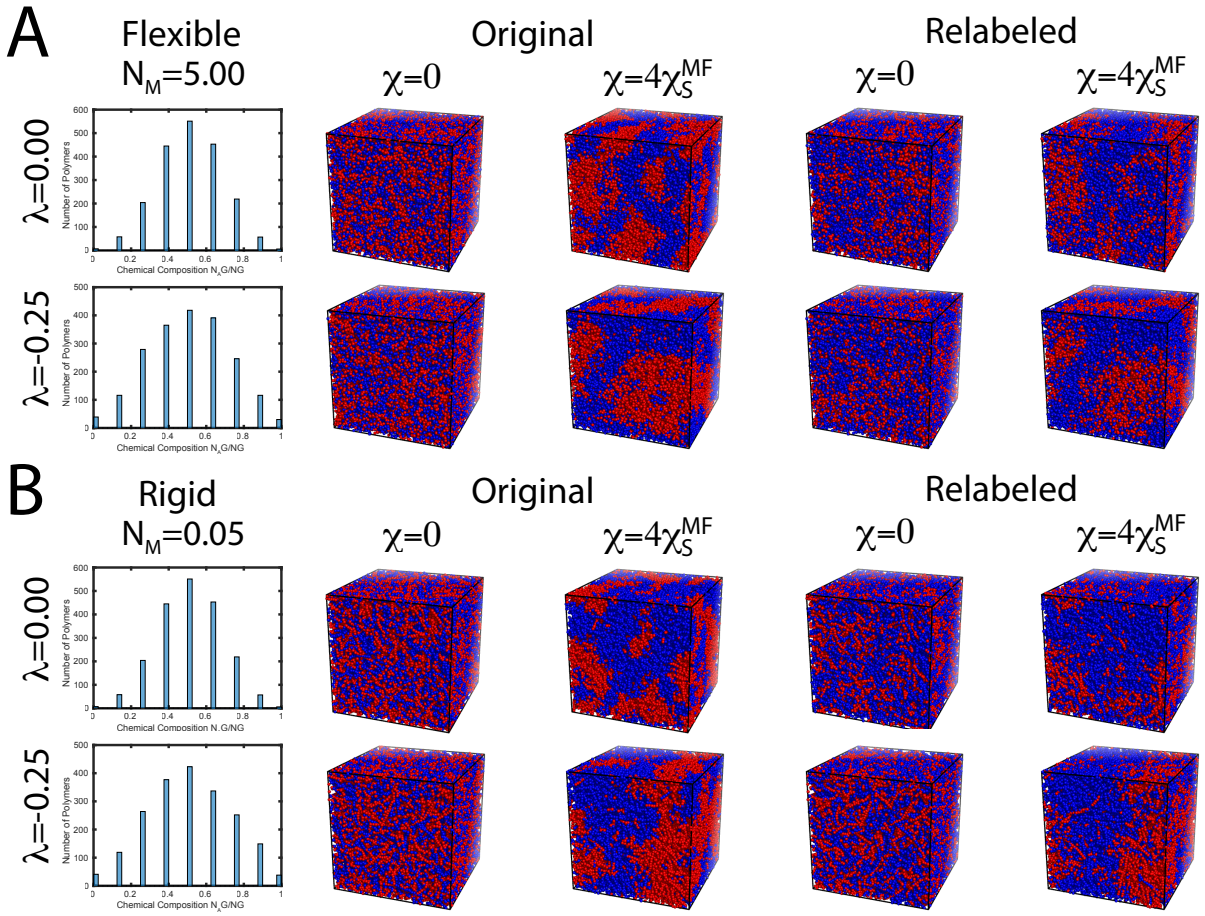

Figure 4: Original and relabeled snapshots of ideal random copolymers with increasing Flory-Huggins parameter χv_M. (First column): Counts of number of chains according to overall chemical composition $N_A G/NG$, where N_A is number of A-type monomers. (Snapshots in top two rows): Flexible random copolymers (N_M = 5.00) composed of beads with original and relabeled chemical identities at λ = 0 and λ = 0.25. (Snapshots in bottom two rows): Rigid, ideal random copolymers (N_M = 0.05, λ = 0) composed of beads with original and relabeld chemical identities.

relabeled identities. By relabeling, we mean 'recoloring' the beads by changing the chemical identity of each submonomer according to the overall chemical composition of the chain. If a chain is composed of equal to or more than half of the beads as A-type beads, then we relabel the chemical identity of all beads as A-type on the same chain, and *vice versa*.

Figure 4 shows the snapshots of polymer melts composed of original and 'relabeled' beads. As the top two rows show, when the Flory-Huggins parameter is raised to four times the mean-field spinodal $\chi = 4\chi_{\rm S}^{\rm MF}$, the chains are locally aggregated according to their

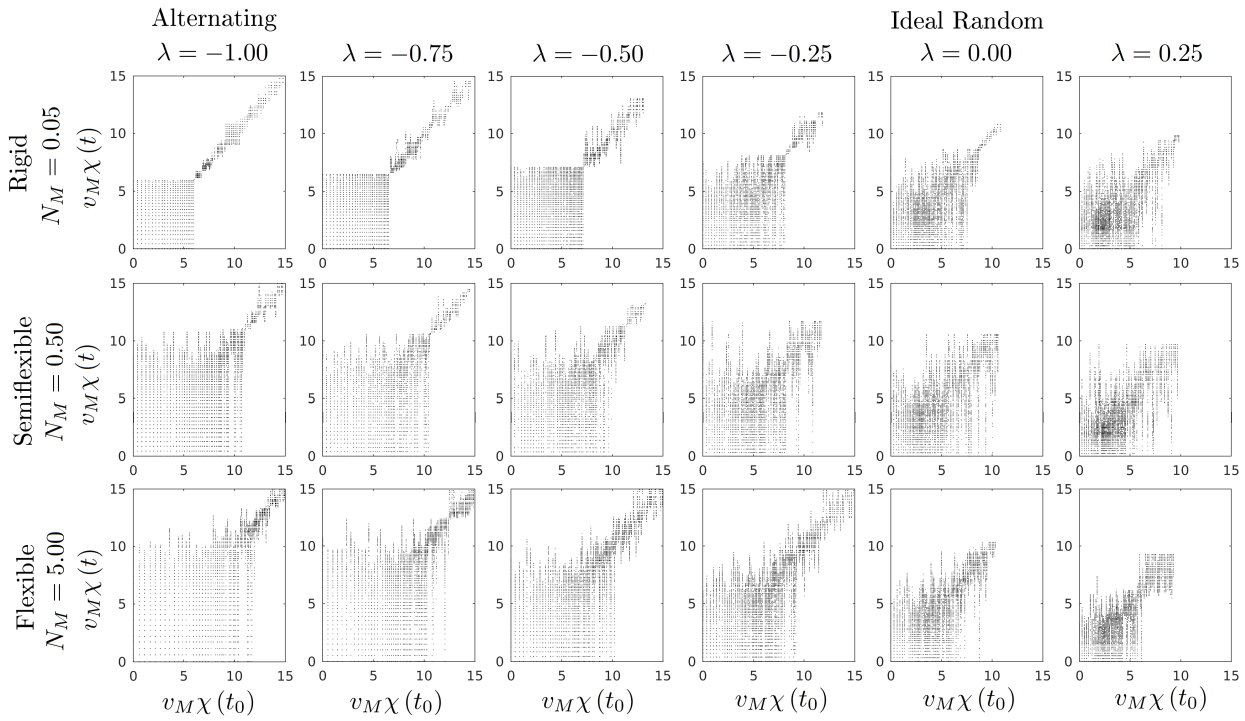

Figure 5: Mixing of replicas by parallel temperting. Each black dot represents that the configuration that had $\chi v_M(t_0)$ at the beginning of data collection visited - at least once - the replica at χv_M at some later time. Each plot is initially diagonal and grows outward. A solid block represents good mixing.

overall chemical composition. The shapes of the new domains of the relabeled beads are also reminiscent of the original snapshots. Specifically, at chemical correlation $\lambda = 0.25$, the spread of chain chemical compositions is larger than ideal random copolymers. In this case, the partition is more visible in the relabeled melts. Likewise, rigid, ideal random copolymers also aggregate according to the overall chemical compositions of the chains. The domains of same-identity relabeled beads are larger since the total sizes of chains are larger than flexible copolymers. This is qualitative evidence of the spatial partition of the chains for formation of multiphases as proposed by Ref.[5]

Replica Coupling Details

In order to efficiently sample the rough energy landscape experienced by a melt of many interacting polymer chains we employ parallel tempering.[6–8] The basic idea of parallel tempering

is to run a Monte-Carlo algorithm on a combined system of multiple non-interacting replicas of the system of interest at different temperatures. A Monte-Carlo move type is introduced which swaps two sub-systems at different temperatures. This allows replicas at lower temperatures to move between local minima by exchanging with replicas at higher temperatures. Rather than parallel couple systems at different temperatures, we couple replicas at different χ values. Because at low χ values our system isn't frustrated and rapidly re-randomizes its configuration, any configuration which traverses from a high to low χ value and back will represent a statistically independent sample. Coupling in χ has the added benefit that it produces results for a tightly spaced set of χ values. Because system configurations are nearly computationally independent they are amenable to parallel implementation.

The effectiveness of parallel tempering is dependent on the choice of χ values to parallel temper over. A good rule of thumb is to space the replicas so that the acceptance ratio is about 20%.[6,9] The probability of exchanging two replicas is given by

$$p = \min\left(1, e^{\Delta\chi V \Delta\langle\phi_A\phi_B\rangle}\right)$$

which can be estimated by

$$p = \min\left(1, e^{-(\Delta\chi)^2 V c_\chi}\right)$$

Because c_χ is a function of χ that is unknown before the start of the simulation, we dynamically adjust each χ such that the probability of exchanging between adjacent χ values is 12-22%. In the case of a first-order phase transition, c_χ has a δ singularity and we are unable to maintain replica exchange across the transition. For this reason our sampling is worse at χ values in the AM phase.

Just because two replicas are exchanging at a reasonable rate does not mean that effective parallel tempering is taking place. Because successive swaps are often far from independent an exhcnage rate of 20% between successive χ values doesn't mean that a configurations can travel by successive swaps from highest to lowest χ values. In Fig. 5 we show the χ

values visited by a configuration during the post initialization period, defined by the final 100 save points ordered by their χ value at the beginning of the period. At low χ values the configurations mix well, corresponding to a block of points which extends to the axes. At high χ, configurations never stray far from their inital χ values, particularly for rigid, alternating polymers. The location of the first-order phase transition is apparent.

Discretization effects

Generally speaking, any numerical methods to find the microstructure of polymeric system relies to some extent on spatial discretization. Likewise, in the field-theoretic Monte-Carlo simulation scheme we used, the spatial discretization to account for chemical incompatibility and melt incompressibility effectively introduces a wavelength cutoff $1/\Delta$ to the Hamiltonian in the continuous field theory. In the continuous field theory, the chemical incompatibility interaction distance is based on the spatial delta function $\delta(\vec{r}_1 - \vec{r}_2)$, which contributes to the structure factor $S(q)$ at all wavelengths. Whereas in the field-theoretic Monte-Carlo simulation, the calculation of interaction energy based on discretized space effectively ignores the effect of chemical incompatibility beyond wavenumber $q \approx 1/\Delta$. Such a wavelength cutoff in the simulation corresponds to ignoring the microscopic length scale contributions to the thermodynamic behavior. In considering the density-density correlations in the mesoscale length scale (on length scales comparable to $1/q^*$) during phase transition, the spatial discretization removes the ultra-violet (UV) divergence (on length scales with small wavelength $1/q$) in the continuous field theory. However, the choice of the cutoff wavelength needs to be justified through renormalization group theory .[10–13] In our simulation, we chose the wavelength cutoff $1/\Delta$ such that we can identify the mesoscale features on the order of wavelength q^* and microscale density fluctuations beyond the wavelength cutoff are ignored. We will qualitatively examine the effect of spatial discretization in the simulation, and leave a more detailed study to a future manuscript.

In the results shown in the manuscript, we chose discretization size Δ = 1.0. To look

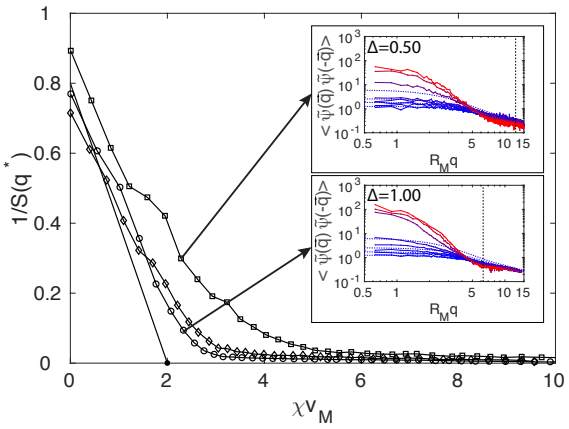

Figure 6: Main panel: Inverse peak intensities of structure factors at different bin discretizations versus Flory-Huggins parameter. ◯: Δ=1, ◇: Δ=2/3, □: Δ=1/2. Insets: Structure factors with bin size Δ=1/2 and 1. From blue to red correspond to the range χ/χ_S^{MF} = 0.0, 0.25, 0.50, 0.75, 1.0, 2.0, 3.0, and 4.0. The dashed lines are obtained from the mean-field theory at χ/χ_S^{MF}=0.0, 0.25, 0.50, and 0.75. The verticle black dashed lines indicate the bin size $q = \pi/\Delta$.

at the effect of bin discretization, we performed simulations of rigid random copolymers (λ = 0.00, N_M = 0.05) with different choices of Δ. Figure 6 shows inverse peak intensities $1/S(q^*)$ versus Flory-Huggins parameter χv_M with $\Delta = 1/2$, 2/3, and 1. The insets in Fig. 6 show the structure factors at $\Delta = 1/2$ and 1, with the dashed lines indicating the length scale of the discretization cutoff $q = \pi/\Delta$. The noise in $S(q^*)$ can be largely attributed to the uncertainty of determining q^* as shown in the insets. Qualitatively, with choice of smaller spatial discretization Δ = 1/2, the structure factors have the same characteristic features as with Δ = 1. However, the inverse peak intensities deviate more from the mean-field theory predictions, since detailed density fluctuations at short wavelengths are included when discretization bins are smaller. Previous work addressed the discretization dependence on χ parameters by matching the free energy of the melt to a mean-field expression near $\chi \approx 0$. [14–16] We implemented this approach and observed that the peak intensities at renormalized χ values do not collapse onto a single curve. This suggests that a simple linear rescaling of χ parameters does not fully address the discretizaiton effects on a wide range of interaction parameters. To fully account for the bin discretization effect, the simulation needs to be

compared with a theory that removes the UV divergence (such as for diblock copolymers in Ref.[17,18]).

References

[1] Kratky, O.; Porod, G. Rontgenuntersuchung Geloster Fadenmolekule. *Recl. Trav. Chim. Pay. B.* **1949**, *68*, 1106–1122.

[2] Saito, N.; Takahashi, K.; Yunoki, Y. *J. Phys. Soc. Jpn.* **1967**, *22*, 219.

[3] Koslover, E. F.; Spakowitz, A. J. Discretizing elastic chains for coarse-grained polymer models. *Soft Matter* **2013**, *9*, 7016–7027.

[4] Koslover, E. F.; Spakowitz, A. J. Systematic Coarse-Graining of Microscale Polymer Models as Effective Elastic Chains. *Macromolecules* **2013**, *46*, 2003–2014.

[5] Nesarikar, A.; de la Cruz, M. O.; Crist, B. Phase transitions in random copolymers. *The Journal of chemical physics* **1993**, *98*, 7385–7397.

[6] Rathore, N.; Chopra, M.; de Pablo, J. J. Optimal allocation of replicas in parallel tempering simulations. *The Journal of chemical physics* **2005**, *122*, 024111.

[7] Sugita, Y.; Okamoto, Y. Replica-exchange molecular dynamics method for protein folding. *Chemical physics letters* **1999**, *314*, 141–151.

[8] Trebst, S.; Troyer, M.; Hansmann, U. H. Optimized parallel tempering simulations of proteins. *The Journal of chemical physics* **2006**, *124*, 174903.

[9] Kone, A.; Kofke, D. A. Selection of temperature intervals for parallel-tempering simulations. *The Journal of chemical physics* **2005**, *122*, 206101.

[10] Wilson, K. G.; Kogut, J. The renormalization group and the ϵ expansion. *Physics Reports* **1974**, *12*, 75–199.

[11] Ohta, T.; Nakanishi, A. Theory of semi-dilute polymer solutions. I. Static property in a good solvent. *Journal of Physics A: Mathematical and General* **1983**, *16*, 4155.

[12] Shankar, R. Renormalization-group approach to interacting fermions. *Reviews of Modern Physics* **1994**, *66*, 129.

[13] Hohenberg, P.; Swift, J. Metastability in fluctuation-driven first-order transitions: Nucleation of lamellar phases. *Physical Review E* **1995**, *52*, 1828.

[14] de la Cruz, M. O.; Edwards, S.; Sanchez, I. Concentration fluctuations in polymer blend thermodynamics. *The Journal of chemical physics* **1988**, *89*, 1704–1708.

[15] Müller, M.; Binder, K. Computer simulation of asymmetric polymer mixtures. *Macromolecules* **1995**, *28*, 1825–1834.

[16] Vorselaars, B.; Stasiak, P.; Matsen, M. W. Field-Theoretic Simulation of Block Copolymers at Experimentally Relevant Molecular Weights. *Macromolecules* **2015**,

[17] Glaser, J.; Qin, J.; Medapuram, P.; Morse, D. C. Collective and Single-Chain Correlations in Disordered Melts of Symmetric Diblock Copolymers: Quantitative Comparison of Simulations and Theory. *Macromolecules* **2014**, *47*, 851–869.

[18] Glaser, J.; Medapuram, P.; Beardsley, T. M.; Matsen, M. W.; Morse, D. C. Universality of block copolymer melts. *Physical review letters* **2014**, *113*, 068302.